Lithospheric Structure in the Pacific Geoid

The determination of the shape of the earth has led to an understanding of the geoidal undulations as they relate to the density distribution on and within the surface of the earth. A spherical harmonic expansion of the gravitational potential everywhere outside of the earth yields, in essence, a decomposition of the geoid field with respect to spatial variation. From this decomposition, the geoid can be divided into the long-wavelength ($\lambda \geq 4500$ km), the intermediate-wavelength ($4500 \geq \lambda \geq 200$), and the short-wavelength ($\lambda \leq 200$ km) contributions. The long-wavelength part of the field is attributed to mantle convection cells extending deep into the mantle, whereas the short-wavelength part is due to uncompensated seafloor topography. On the other hand, the source of the intermediate wavelengths of the geoid is not well understood. Investigators have speculated that these intermediate geoid undulations are perhaps due to shallow, small-scale mantle instabilities, but a correlation has been observed with the structure of the lithosphere.

We have been studying the high degree and order (n,m > 12,12) SEASAT geoid in the central Pacific as it correlates with the structure of the cooling lithosphere. Relative changes in lithospheric plate age across major fracture zones in relatively young ($\leq$ 80 Ma) seafloor frame the east-west trending pattern formed by the geoid anomalies (Figure 1). The separation of the major fracture zones is ~ 1000 km, whereas the dominant wavelength of the geoid field is

(NASA-CR-174155) LITHOSPHERIC STRUCTURE IN THE PACIFIC GEOID Semiannual Report (Johns Hopkins Univ.) 5 p HC A02/MF A01 CSCL 08E

N85-13365

Unclas
G3/43 24572

~ 2000 km in the north-south direction.

Investigators customarily remove the effects of regional lithospheric thermal subsidence from bathymetry to expose anomalies in depth, the so-called residual depth anomalies. This field removal in bathymetry corresponds to removal of some of the low degree and order (n,m < 12,12) geoidal components, and the step-like structure across fracture zones is also removed. We have, instead, removed the regional thermal subsidence from the bathymetry by subtracting a mean subsidence surface from the observed bathymetry. This produces what we are calling a residual bathymetry map (Figure 2) analogous to the usual residual depth anomaly maps. The residual bathymetry obtained in this way then contains shallow depths for young seafloor, and larger depths for older seafloor, thus retaining the structure of the lithosphere while removing the subsidence of the lithosphere. This is the operation we have performed on the bathymetry data for the purpose of yielding a transfer function between the geoid field and the bathymetry field. However, a better way to proceed is to expand the bathymetry field in terms of spherical harmonics, and then remove the coefficients up to, and including, degree and order 12. By doing this, we are left with a high degree and order bathymetry field which has been treated identically to the geoid, thus eliminating possible ambiguities due to model field removal.

In order that sub-lithospheric density variations be revealed with the geoid, the regional geoid anomalies (~ 2 m) associated with bathymetric variations, must first be removed. We have used spectral techniques to generate a synthetic geoid (Figure 3) by filtering the residual bathymetry assuming an Airy-type isostatic compensation model. We have assumed a value of 100 km for the thickness

of the lithosphere, and have also assumed the plane approximation to be valid. The resulting field fairly closely resembles in pattern the observed geoid of Figure 1, but the amplitudes are different, and may yet need to be adjusted through the depth of compensation and density structure. It is, nevertheless, clear that this field due to lithospheric structure may be a major component of the geoid in this region.

We have obtained and unbiased estimate of the admittance, and a comparison with model admittances shows that, for the region under study, no single compensation mechanism will explain all of the power in the geoid. Our values of the admittance for the shorter wavelengths ($\lambda < 450$ km) agree with the values obtained by Sandwell & Poehls (1980) for a similar region in the Pacific assuming an Airy model. The longer wavelengths do not agree with the Airy model, nor do they agree with the thermal compensation model. This may most likely be due to the fact that the spectral contributions from the Hawaiian swell and from the regional Pacific bathymetry are indistinguishable in the frequency domain. Nevertheless, because topographic features are mainly coherent with the geoid, to first order an isostatically compensated lithosphere cut by major E-W fracture zones accounts for most of the power in the high degree and order SEASAT geoid in the central Pacific.

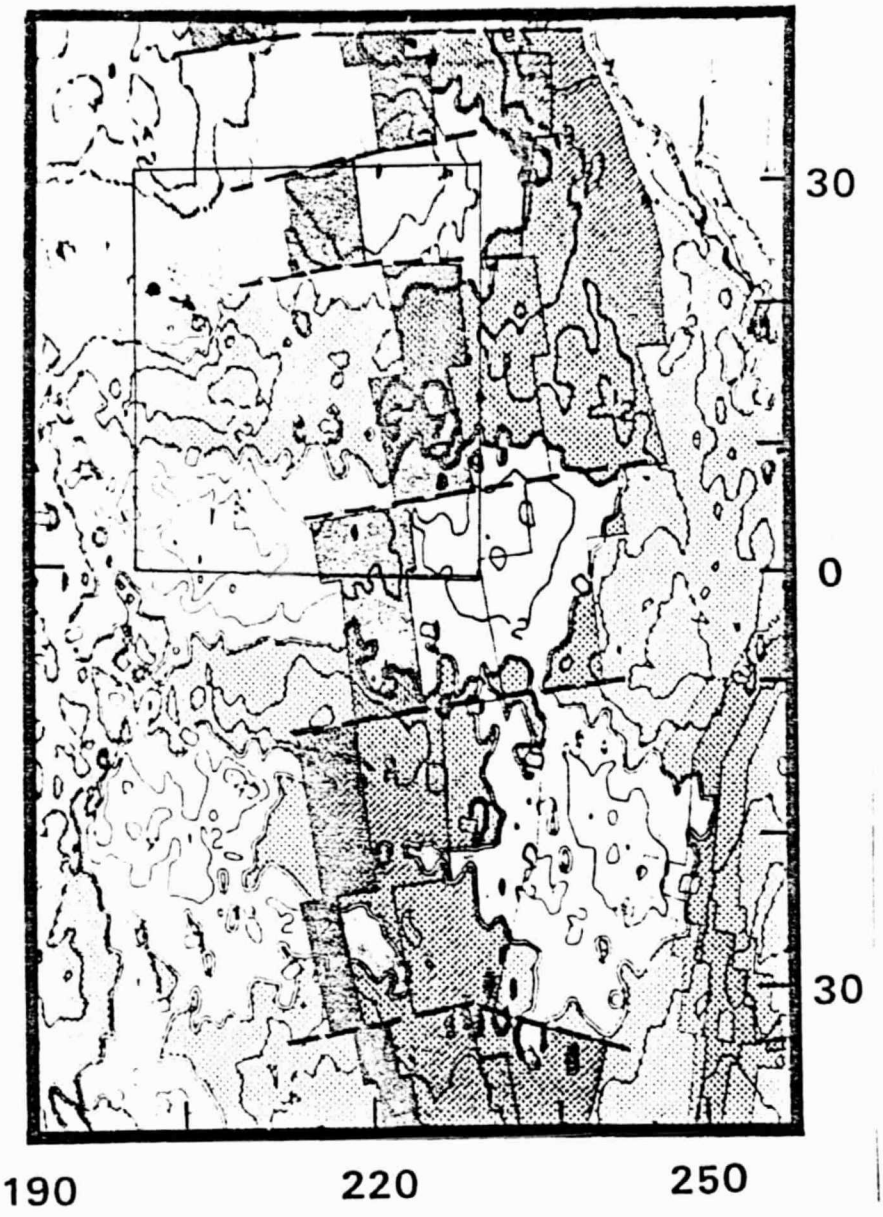

Fig. 1. The SEASAT geoid superimposed on the map of the age of the ocean basins of Pitman et al. (1974). Major fracture zones with large offsets have been marked with dashed lines. From north to south, these fracture zones are Mendocino, Murray, Molokai, Clipperton, and Marquesas and the last is apparently unnamed. These fracture zones frame the pattern of geoid anomalies, and there is a correlation between regions of relatively young seafloor and positive geoid anomalies.

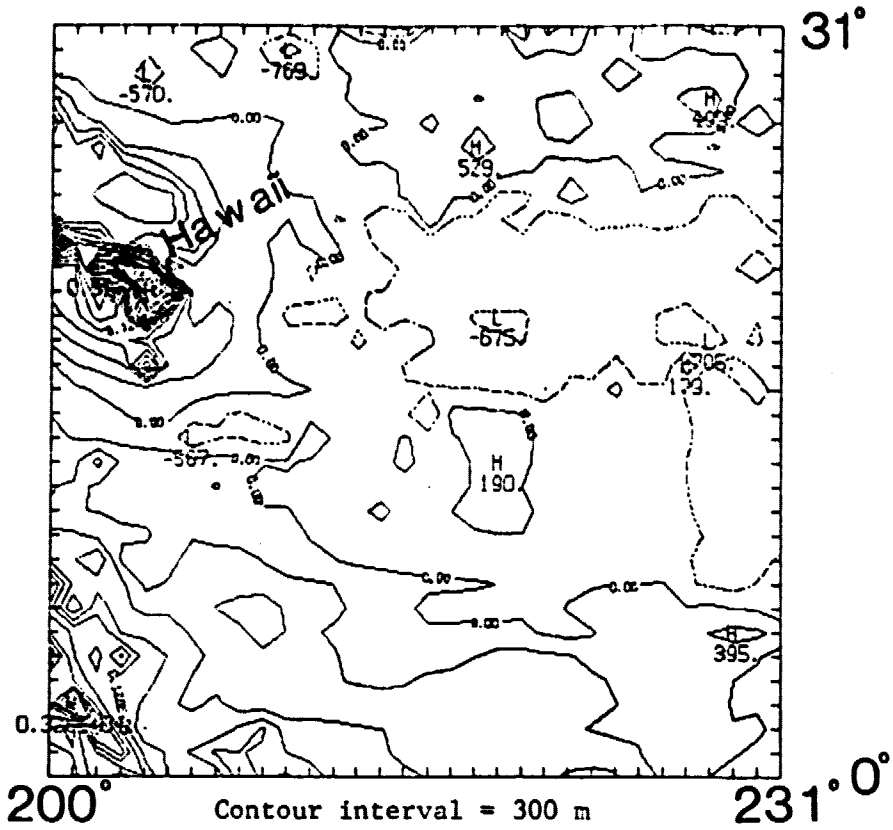

Fig. 2. The residual bathymetry obtained by removing a mean thermal subsidence surface from the observed bathymetry. Large positive values occur over shallow, young seafloor, and large negative values over deep, older seafloor.

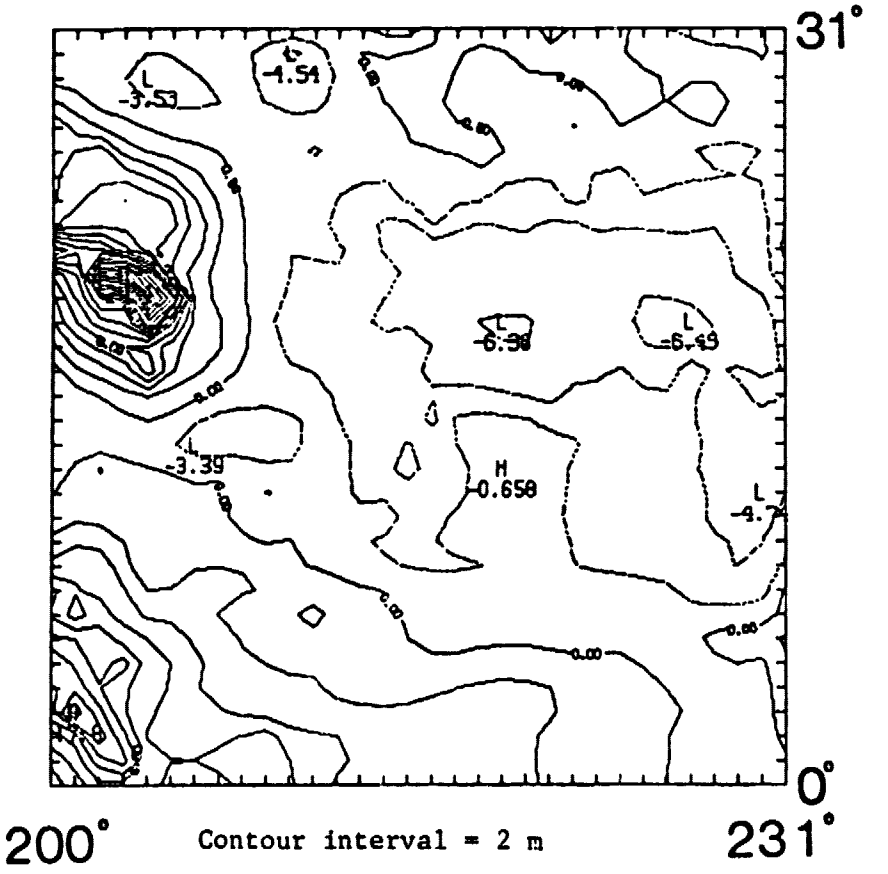

Fig. 3. The synthetic geoid obtained by filtering the residual bathymetry in figure 2 through an Airy-type isostatic compensation model.